Poly(2-isoproprenyl-2-oxazoline)-based reactive hydrophilic crosslinked nanofiber networks as basis for colorimetric continuous meat freshness monitoring sensors

Ronald Merckx,[1] Jana Becelaere,[2] Ella Schoolaert,[2] Olmo Frateur,[2] Meike Nicole Leiske,[1] Daniël Peeters,[1] Florica Adriana Jerca,[3] Valentin Victor Jerca,[3,] Karen De Clerck,[2,]* Richard Hoogenboom[1,]**

[1]Supramolecular Chemistry Group, Centre of Macromolecular Chemistry (CMaC), Department of Organic and Macromolecular Chemistry, Ghent University, Krijgslaan 281-S4, 9000 Ghent, Belgium. E-mail: richard.hoogenboom@ugent.be

[2]Centre for Textile Science and Engineering, Department of Materials, Textiles and Chemical Technology, Ghent University, Tech Lane Science Park 70A, 9052 Ghent, Belgium. E-mail: Karen.DeClerck@UGent.be

[3]Smart Organic Materials Group, "Costin D. Nenitzescu" Institute of Organic and Supramolecular Chemistry, Romanian Academy, Spl. Independentei 202B, 060023, Bucharest, Romania. E-mail: victor.jerca@ccocdn.ro

KEYWORDS: post-polymerization modification; poly(2-isopropenyl-2-oxazoline), nanofibers sensors; food monitoring

ABSTRACT: Global food waste is a cross-cutting issue that ranges from agricultural production to storage in households and leads up to the loss of one third of the produced food products. Although the currently depicted static expiry, best-by and due-by date provide accurate information on when to consume the food product, this time indication is only valid under ideal storage conditions. Therefore, there is a stringent need for easy-to-use sensor applications that allow continuous monitoring of the food freshness. This work showcases a straightforward and effortless approach to obtain highly porous crosslinked water-stable, reactive hydrophilic nanofiber membranes based on electrospinning of poly(2-isoproprenyl-2-oxazoline) (PiPOx) with succinic acid as crosslinker. Subsequent thermal treatment of the produced succinic acid containing PiPOx nanofiber networks generated sufficient crosslinking to preserve the fibrous morphology in an aqueous environment while retaining the hydrophilic character of the scaffold. The remaining 2-oxazoline side chains of PiPOx are stable at room temperature but provide reactivity for post-crosslinking modification with carboxylic acid containing compounds as exploited here for continuous food monitoring by incorporating acid-functionalized dyes yielding a colorimetric sensor for biogenic food spoilage indicators, such as thiol and amine-containing small molecules.

1. Introduction

Establishing the quality of food products, especially protein-based foods (e.g. fish and meat) is anything but trivial. The first concern that makes the freshness assessment of food essential is the need to reduce the risk of food poisoning to a minimum, which originates from the microorganisms (bacteria, viruses, or parasites) growing on spoiled food. Foodborne diseases could result from consumption after the expiration date, lousy storage, adverse events along the supply chain, or the consumer's improper manipulation. Yearly in Europe, 23 million people are affected by food poisoning.[1] Secondly, but no less critical, freshness assessment is mandatory to reduce unjustified food waste as safety margins on expiry dates leads to major disposal of still edible food. [2] Food quality control systems include specific analytical measures that provide reliable data, but are limited to control agencies, requiring long-time analyses, equipped laboratories, and trained personnel. Therefore, there is a stringent need for solutions that can assess the quality of a single piece of meat/fish based on simple systems of low cost and whose output is easy to comprehend. Consequently, developing such continuous monitoring devices has received significant attention.[3] The largest category of systems is focused on collateral properties, indirectly related to food freshness. Devices aimed to control the cold chain's maintenance,[4] or the modified atmosphere's integrity for the food packed under CO_2 are a few examples.[5] However, the response obtained by these systems provided an irrefutable conclusion on the freshness of the food product, the sophisticated control of the meat's color or its headspace composition required apps or trained people and are nowhere near the envisioned instrument-less and straightforward responses. Moreover, all electronic noses, tongues,[6-8]or devices require a complex algorithm to assess the food freshness.[9] Undoubtedly, the colorimetric sensors present the best candidates for the development of food assessment due to their simplistic color change and easy read-out. These

could be placed in the tray over the meat and detect the shift in volatile compound composition from safe to hazardous conditions by an on/off response signal. Many proposals in the literature exploited this principle, mainly based on pH indicators.[10-16] However, the documented results cannot pinpoint the complex deterioration of the food product. During food spoilage, a more complex mixture of analytes is formed, which is not included in the purely pH-focused analysis.

In principle, for each degradation step, the volatile by-products formed during spoilage exhibit different acid-base behavior, resulting in changes in the meat sample's headspace composition.[17] In any muscle converted to meat, anaerobic glycolysis takes place during which the glycogen is hydrolyzed into lactic acid, resulting in an acidity decrease towards pH 5-6. After that, bacterial decomposition of the substances occurs. At this step, despite the wide variety of microorganisms and substrates, all proteinaceous food spoilage process are rather similar, mainly related to the classes of precursors commonly present in these matrices. Firstly, sugars and fats are degraded by bacteria, producing molecules that can migrate from the meat to the headspace. In this phase, volatile organic compounds (VOCs) produced include ethanol, 3-methyl-1-butanol, and free fatty acids, mainly acetic acid. Until this phase, protein foods are considered safe products. However, to our knowledge, no sensing devices were developed exhibiting recognition to this stage. From the moment when glucose and its direct metabolites are depleted, the catabolism of proteins start, producing an assortment of amines, biogenic amines, sulfur compounds, and thiols. For example, sulfur compounds such as methanethiol originate from proteins containing amino acids such as cysteine. As spoilage proceeds, the discoloration and production of odor mark this stage. By now, the produced by-products are toxic, and meat consumption at this stage could be a severe hazard. The overwhelming majority of papers that proposed colorimetric (nanofibrous) sensors merely

focused on dye-doping to detect the presence of biogenic amines in the headspace, neglecting most of the other metabolites.[10, 12, 14, 18-21]

A first, main issue with the reported dye-doped sensor systems is the possible leaching of the analyte-sensitive dye from the material, resulting in loss of sensitivity or, even worse, possible toxicological responses when entering the food product. Therefore, most of the literature research focuses on reducing this dye leaching by various, often tedious, chemical modifications or incorporating additives.[12, 22-25] To completely suppress dye-leaching from the designed materials, the covalent incorporation of the desired functionality onto a base material is required either during or after the fabrication. A second issue with the currently developed systems is sensitivity. Due to the small amounts of metabolites formed during the initial stages of the spoilage process, a sensor material with high sensitivity is desired. Typically, materials providing this characteristic are highly porous, making it easier for the analyte to reach the sensor's active component. Therefore, if functionalized with the correct dyes, nanofibers networks with their characteristic high surface-to-volume ratio lend themselves to be a suitable candidate for developing a food sensor with a colorimetric read-out.

Electrospinning, first introduced by Formhals in 1934[26] has been widely adopted as an effective and versatile technique to produce fibers with a diameter ranging from nano to micrometres.[27, 28] A large variety of synthetic and natural polymers have been electrospun to form nanofiber systems used in fields such as tissue engineering,[29-31] protective clothing,[32, 33] environmental protection,[34, 35] sensors,[36-38] optics,[39] as well as water filtration and purification.[40] The wide applicability of such nanofibrous non-woven materials is largely due to the remarkable properties of the nanofiber systems including a high surface area to volume ratio, tunable porosity and the ability to manipulate the nanofiber composition to acquire the desired properties and function.[41]

Solvent electrospinning is the most commonly applied technique for the production of such nanofibers.[41] For future industrial applications of electrospinning as well as for biomedical applications of the nanofibers, the 'green-factor' of the electrospinning solvent and its ecotoxicity are becoming indisputable requirements for effective valorisation.[42] Consequently, the use of green, non-toxic solvents, such as water and ethanol, becomes increasingly important. Over the past decade, several reports were published on the electrospinning of naturally derived, water-soluble biopolymers including collagen, silk fibroin and gelatin.[43-45] Moreover, various biocompatible and water soluble synthetic polymers, such as poly(vinyl alcohol) (PVA),[46-48] poly(ethylene oxide) (PEO),[49-51] poly(vinylpyrrolidone) (PVP),[52] poly(2-oxazoline)s,[53] and poly(*N*-isopropylacrylamide) (PNIPAM) were used to prepare nanofibers from aqueous solvent systems.[54, 55]

Although the green electrospinning of water-soluble polymers provides a sustainable way to produce hydrophilic nanofiber materials, the lack of water stability precludes their use in humid environments or aqueous media representing a major disadvantage and limitation. Therefore, various procedures were developed to increase the dimensional stability of hydrophilic nanofibers by crosslinking, which, however, comes with some drawbacks, including time-consuming multi-step modification procedures, toxic reagents, tedious purification of polymeric precursors, and more difficult processing.[56-58] Typically, crosslinking of electrospun nanofibers is performed after the electrospinning process as precrosslinking can only be done to a minor extend to retain processability.[56] For example, Li and coworkers reported the photocrosslinking of benzophenone functionalized poly(2-ethyl-2-oxazoline) (PEtOx) nanofibers.[56] The photocrosslinking process significantly increased the water stability of PEtOx nanofibers; however, the modification procedure was performed in two steps by partially hydrolyzing PEtOx followed by a reaction with

4-benzoylbenzoyl chloride and involved the use of harmful reagents. Several other crosslinking strategies, including ultraviolet irradiation or dehydrothermal treatment, and use of crosslinking agents such as dicumyl peroxide, glutaraldehyde, and citric acid have been reported for increasing the hydrolytic stability of various polymeric nanofibers.[42, 59-61] However, the production of water-stable, hydrophilic and biocompatible nanofibers remains subject to further optimization, e.g. by exploring more facile and eco-friendly production methods. Consequently, finding and investigating other alternative polymers represent the focus of ongoing research.[62, 63]

This study focuses on development of a continuous food monitoring system based on dye-functionalized hydrophilic crosslinked nanofibers consisting of poly(2-isoproprenyl-2-oxazoline) (PiPOx), which was recently demonstrated to be a biocompatible, hydrophilic polymer[64-66] The polymer can be synthesized from the 2-isoproprenyl-2-oxazoline (iPOx) monomer using different polymerization methods, i.e. free radical,[67] reversible addition−fragmentation chain-transfer,[68] atom transfer radical,[69] group transfer,[70] and anionic polymerization[64, 71] with the retention of the 2-oxazoline ring as reactive side-chain functionality. The resulting polymer is a versatile, functional polymer that has been used in the synthesis of various (multi)functional materials, including hydrogels for water purification[72] and for ophthalmic applications,[64] molecularly imprinted polymers for drug delivery[73] ultra-high strength hydrogels[74] photonic applications[75] and optical and temperature sensors.[65, 67] The advantages of this platform compared to other existing polymers such as PVA, PVP or PNIPAM reside in the hydrophilicity, biocompatibility and stability under physiological conditions of the polymer in combination with the straightforward post-polymerization modification reaction of the 2-oxazoline side-chains with (di)carboxylic acid groups at elevated temperatures[66, 76]. Therefore, PiPOx represents an excellent candidate as a base material for the synthesis of reactive crosslinked hydrophilic nanofiber networks, which to the best

of our knowledge, has not been previously reported in the literature. Furthermore, PiPOx offers the great advantage of in situ crosslinking, which can be facilitated by the incorporation of a biobased, non-toxic, cost-efficient and readily available dicarboxylic acid such as succinic acid followed by curing the nanofibers at elevated temperature. The resulting crosslinked hydrophilic nanofiber networks can be used for post-processing modification by soaking in a solution with a carboxylic acid containing solution followed by heating. Although the name of this polymer might suggest at first sight that it belongs to the well-known class of poly(2-oxazolines) (PAOx), one must emphasize that the chemical structure of PiPOx does not resemble the pseudo-polypeptide structure of PAOx and can not be regarded as an analogue, while the properties and chemical reactivity are different as well. Consequently, processing of PiPOx into (nano)fibers is not a simple optimization of the electrospinning process as previously used for PAOx. Moreover, the PiPOx (nano)fibers could potentially open up new research directions and applications due to their post-modification possibilities as already demonstrated in the literature for PiPOx hydrogels.[64, 72, 74, 77]

In the present study, a straightforward method is introduced to prepare dye-functionalized hydrophilic crosslinked nanofiber networks for continuous food monitoring. Therefore, PiPOx nanofiber networks were fabricated by electrospinning a solution of PiPOx homopolymers blended with succinic acid as a crosslinker. The influence of the processing parameters such as flow rate, voltage, and polymer concentration on the morphology of the resulting nanofibers was systematically investigated as well as the post-fabrication crosslinking. The formed PiPOx nanofibers with a porous and uniform morphology before and after crosslinking were characterized using scanning electron microscopy (SEM), Fourier transform infrared (FTIR) spectroscopy, and dynamic vapor sorption gravimetry (DVS). We report that the fabricated nanofibrous networks can effectively absorb water without drastic changes of the morphological structure, indicating its

potential as versatile hydrophilic crosslinked nanofiber network for applications such as colorimetric sensors, fiber-optics and energy transfer membranes. Within this work, we demonstrate the straightforward post-processing modification of these reactive hydrophilic crosslinked nanofibers with various carboxylic acid functionalized dyes for colorimetric detection of thiol and amine containing analytes for food spoilage detection. The potential of this system is shown by providing a proof of concept for spoilage detection of cod fish.

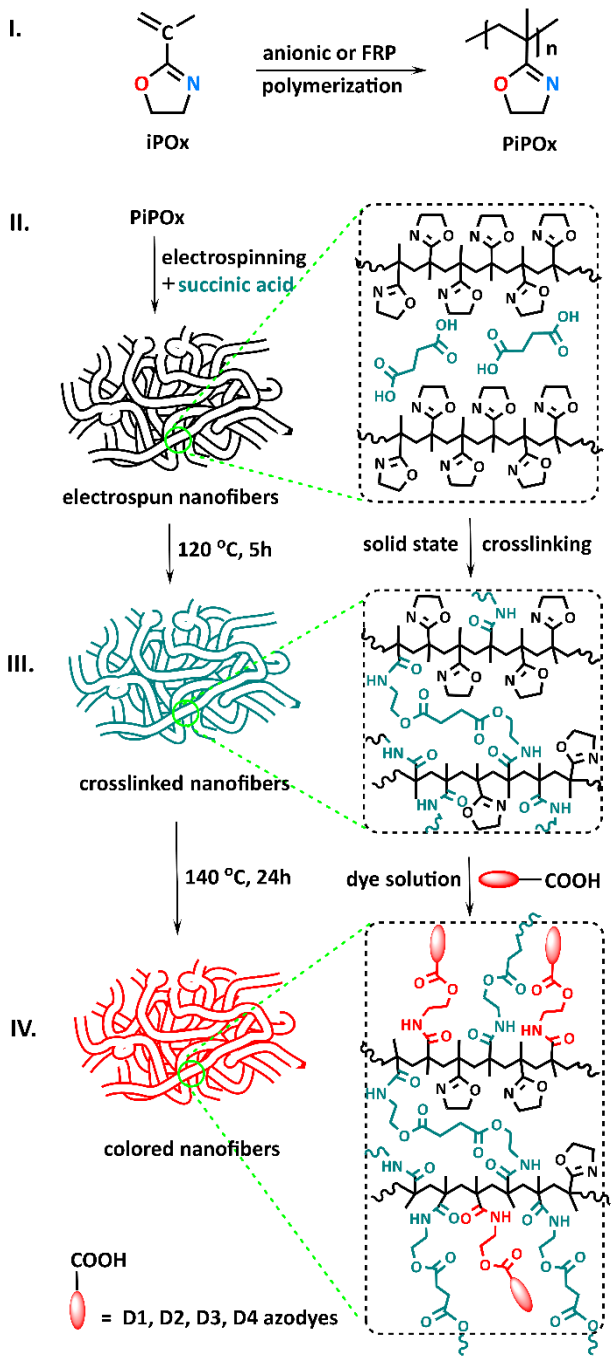

Scheme 1. Synthesis of PiPOx based colorimetric sensor. (I) Synthesis of PiPOx by anionic or free radical polymerization (FRP); (II) Electrospinning process of PiPOx; (III)Crosslinking of PiPOx electrospunn nanofibers; (IV) Attachment of the sensing units to obtain the final colourimetric sensors.

2. RESULTS AND DISCUSSION

2.1. Synthesis and characterization of the PiPOx polymers.

As it was envisioned that a continuous food monitoring platform would be easily accessible through the use of hydrophilic crosslinked PiPOx nanofibers, we first focused our attention on the solvent electrospinning of PiPOx, which was not previously reported in the literature. The processing conditions, process stability, and resulting fiber morphology were considered when investigating the electrospinnability of PiPOx. We focused our efforts on determining the influence of polymer-related parameters, such as molecular weight and dispersity, and processing parameters, including solution viscosity and concentration, on electrospun fiber formation.

The living anionic polymerization (LAP) of 2-isopropenyl-2-oxazoline results in polymers with highly defined characteristics, albeit at the cost of limited scalability due to heat transfer issues and strict processing conditions. Therefore, we evaluated the solvent electrospinning of PiPOx prepared by LAP as well as free radical polymerization (FRP) as it is more straightforward and easier scalable. Nevertheless, one must consider that the LAP of iPOx proceeds with an almost quantitative yield, while the synthesized FRP polymers were obtained with lower yields (61 %). However, the main difference between the two polymerization methods lies in their control. The scalable FRP effortlessly provides PiPOx with high molar mass values and broad polydispersities[67, 78] while LAP[65, 71, 79] provides access to PiPOx with controlled molar mass and narrow dispersity. [65 65 65 64 63 63 63 6363]

A series of PiPOx homopolymers with degree of polymerization ranging from 150 to 315 was synthesized via LAP and FRP. The characteristics of the polymers are listed in Table 1 and their corresponding SEC traces are given in Figure S1.

Table 1. Structural characterization and characteristic properties of the synthesized PiPOx homopolymers.

Polymer Code	Synthesis method	M_n (kDa)[1]	M_w (kDa)[1]	Đ[1]	R_h (nm)[2]	R_g (nm)[3]	c*(g/mL)[4]	c* (wt%)[4]
A150	LAP	15	17.1	1.14	3.2	3.7	0.137	12.5
A222	LAP	22	24.6	1.12	3.8	4.3	0.124	11.3
A315	LAP	33	37.8	1.15	4.6	5.3	0.103	9.4
F300	FRP	36	53.3	1.48	5.6	6.4	0.09	8.2

[1]Determined using SEC-LS in DMAc (SI)

[2]Determined from DLS measurements at 25 °C in DW/EtOH (1:1 wt/wt)

[3]Estimated from R_h using the Kirkwood–Riseman theory

[4]Critical overlap concentration determined in H_2O/EtOH (1:1 wt/wt)

Well-defined PiPOx homopolymers (A150, A222 and A315) with a controlled average molar mass and narrow dispersity of Đ ≤ 1.15 were obtained by LAP (Table 1), while the FRP (F300) polymer showed a much broader dispersity (Đ = 1.48) and significantly difference between M_w and M_n, characteristic to FRP processes.

2.2. Optimization of the electrospinning process.

To reduce the number of experiments and minimize the amount of polymer used, in view of the special reaction conditions required for the LAP, we first determined the theoretical critical overlap concentration (c*) (see Table 1). The knowledge of the c* allows a priori prediction of polymer concentration range needed for successful electrospinnability without having to perform a solution

viscosity study. The critical overlap concentration (c*) of the PiPOx polymers in H_2O/EtOH (1:1 wt/wt) was estimated by the following equation:[80]

$$c^* = \frac{3 \cdot M_w}{4\pi \cdot R_g^3 \cdot N_{Av}} \qquad (1)$$

Where M_w is the weight average molecular weight in g/mol, N_{Av} is the Avogadro number and R_g is the radius of gyration. The R_g in a good solvent can be estimated using the Kirkwood–Riseman theory from the hydrodynamic radius (R_h) according to the below equation:

$$R_g = \frac{R_h}{0.875} \qquad (2)$$

The R_h can be easily determined from dynamic light scattering measurements. As expected, the c* decreases with increasing molecular weight (Table 1). PiPOx with higher molecular weight possesses a higher hydrodynamic volume, thus requiring a lower concentration to overlap. Considering the c* values obtained, polymeric solutions were made in H_2O/EtOH (1:1 wt/wt) at different concentrations higher than c* (e.g., 15, 20, 25 and 30 wt%) to span the semi dilute unentangled and entangled regimes. The processing parameters such as the applied voltage, solvent ratio and the feed rate were adjusted to optimize the electrospinning process using the polymers **A150**, **A222** and **A315**, as summarized in Table S1. These nanofiber diameters were obtained at a feed rate below 1 mL/hr and an applied voltage of 20 kV. Finally, for the polymer F300 the H_2O/EtOH solvent composition was also varied.

Prior to electrospinning the viscosity of these solutions was measured using a rheometer. All the samples displayed a Newtonian behavior within the investigated shear rate interval (Figures S3 and S4). The zero shear viscosity (η_0) was calculated as the slope of the plot of the shear stress-shear rate data in the range 0-100 s^{-1}.

The specific viscosity at each concentration was calculated using the equation below:

$$\eta_{sp} = \frac{\eta_0 - \eta_s}{\eta_s} \qquad (3)$$

where η_0 is the zero-shear viscosity determined for every concentration from Figures S3 and S4 and η_s is the solvent viscosity (2.033 mPa·s).

The η_{sp} is plotted against polymer solution concentration to determine the entanglement concentration (c_e) (**Figure 1**a). The transition between semi-dilute unentangled to the semi dilute entangled regime is observed as a change in the slope. Although c_e cannot be determined with sufficient accuracy due to the limited number of data points one can visually observe that the c_e is in the region of 20 to 25 wt %. Intuitively, one expects that increasing the molar mass of the PiPOx results in a lower c_e value.

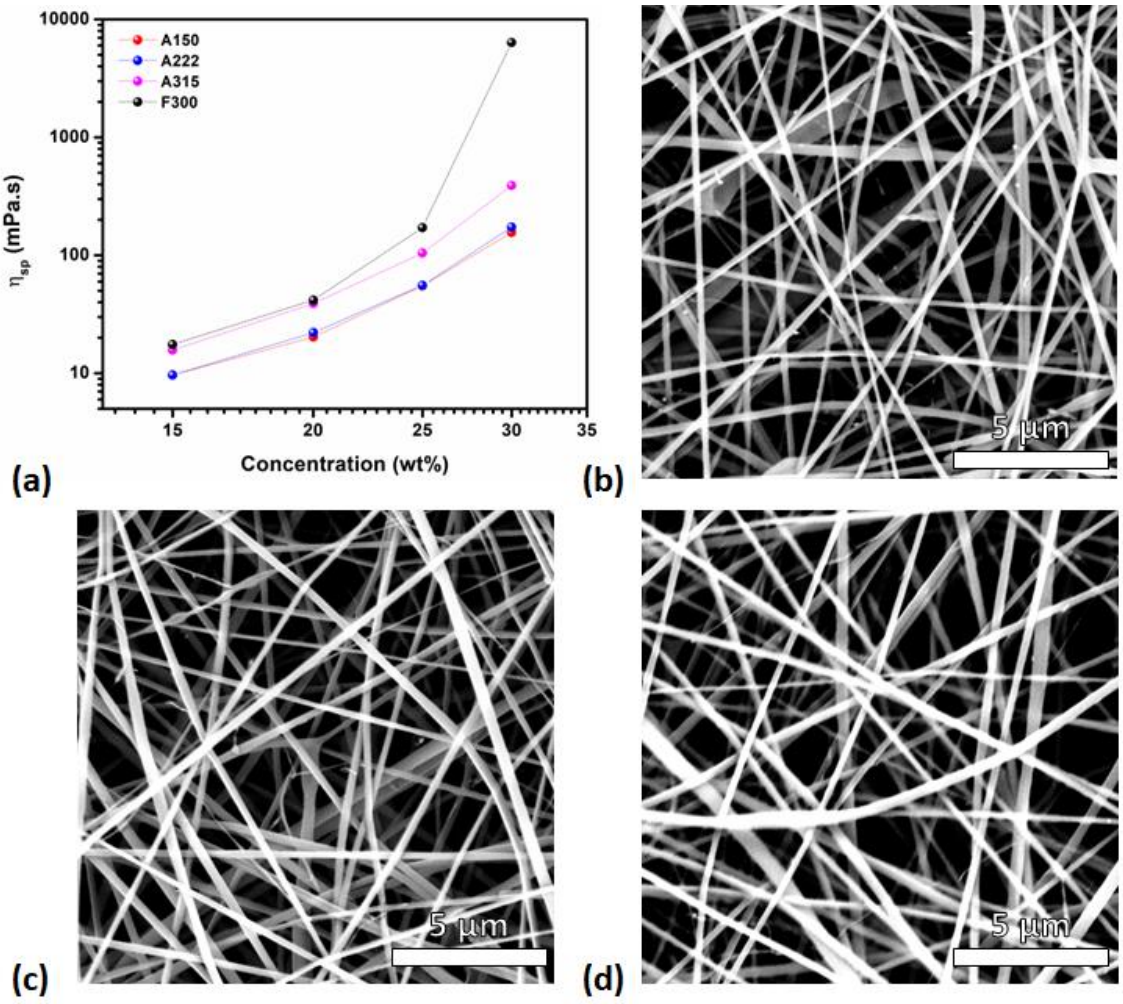

Figure 1. a) Rheological characterization of all polymers at different polymer concentrations in EtOH:H_2O (1/1) mixtures. b-d) Scanning electron microscopy analysis of the fabricated A150, A222 and A315 membranes at 25 wt% evidencing the nanofiber formation.

Subsequently the electrospinnability of various PiPOx solutions was tested. Typically, the fiber morphology changes from beaded fibers to uniform fibers upon increasing the concentration and consequently the viscosity of the polymer solution (**Figure 2**).[81] Electrospinning of 15 or 20 wt% A150, A222, and A315 polymer solutions, that are below c_e, resulted in the formation of polymer beads, as expected, indicating insufficient chain overlap (**Figure 2 and Figure S2**).

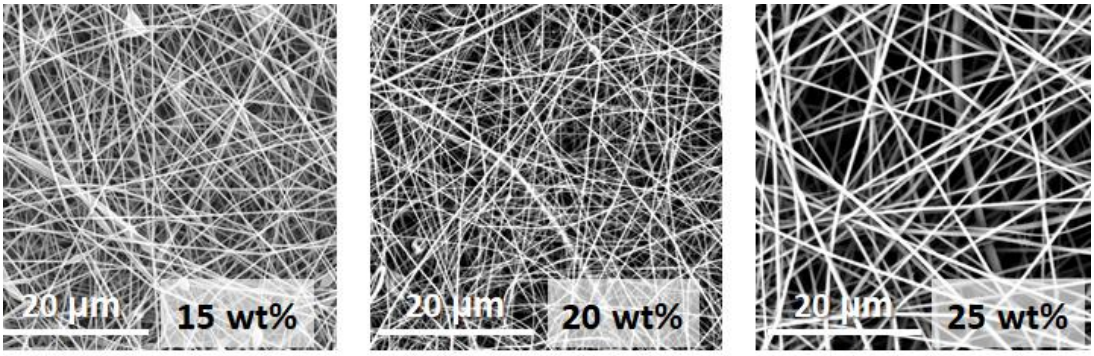

Figure 2. Scanning electron microscopy analysis of the fabricated F300 membranes at three different polymer concentrations.

Further increasing the polymer concentration resulted in the formation of uniform, bead-free nanofibers, whereby an optimum fiber diameter was found at 25 wt% polymer in a H_2O/EtOH mixture (1:1 wt/wt) for all PiPOx polymers obtained by anionic polymerization (**Figure 2**). At a concentration of 25 wt%, all materials had a fiber diameter below 500 nm without any significant deviations between the different chain lengths (Table S1), suggesting that increasing the DP from 150 to 330 has only a minor effect on the fiber formation process (**Figure 1**b-d). In all cases, the fiber diameter increased, and diameter uniformity decreased upon increasing the solution concentration to 30 wt%, further indicating that the viscosity of the solutions becomes too high for controlled electrospinning. PiPOx-F300 also showed bead formation at 15 wt% concentration in H_2O/EtOH (1/1 wt/wt), whereas stable fibers were already obtained at lower concentration, that is 20 wt%, compared to PiPOx-A315, due to the higher molar mass of the PiPOx-F300 (M_w = 53.3 kDa compared to Mw = 37.8 kDa). As the concentration of PiPOx-F300 was further increased the fiber diameter increased as well, up to the point where the 30 wt% solution was no longer electrospinnable due to increased viscosity leading to droplet formation at the needle instead of a stable Taylor cone. The optimal solution viscosity, regardless of PiPOx type and DP was found to be in the range 100 to 300 mPa·s (Figures S3-S4 and Table S1).

The SEM analysis and the resulting fiber diameter data in **Figure 3** and table S1 indicated a stable spinning process, resulting in the formation of nanofibers with a diameter below 500 nm when 25 wt% solution PiPOx-A was used (Table S1). However, electrospinning a 25 wt% solution of PiPOx-F300 resulted in the formation of fibers with higher diameter, that is 736 ± 109 nm (Table S1), due to the increased viscosity of 25 wt% PiPOx-F300 which is 1.6 times higher than the viscosity of 25 wt% PiPOx-A315 (**Figure 3**a). Well-defined nanofibers from PiPOx-F300 were obtained upon lowering of the concentration to 20 wt%, yielding diameters of 458 nm ± 91 nm as illustrated in **Figure 3**b.

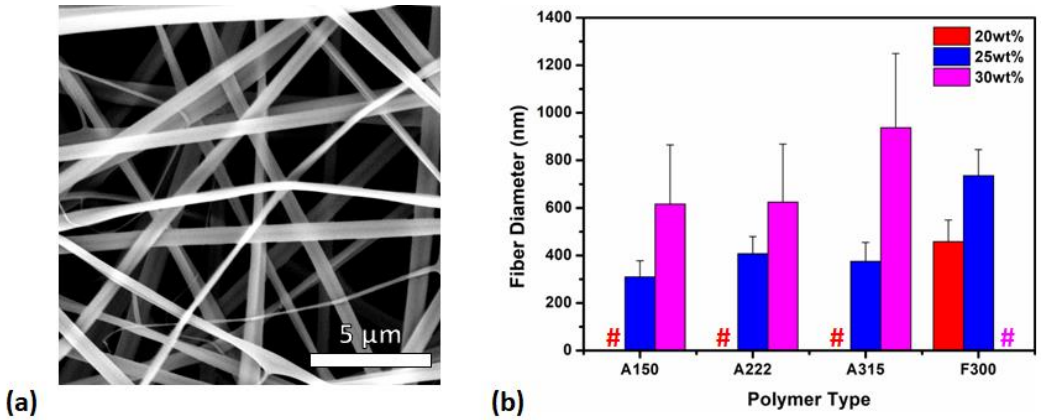

Figure 3. a) Scanning electron microscopy analysis of the fabricated F300 membranes evidencing the nanofiber formation at 25 wt%. b) Overview of the results obtained for electrospun nanofibers (20–30 wt%) from PiPOx synthesized by both anionic and free radical polymerization. Hashes indicate unsuccessful electrospinning experiments depicting bead formation.

To determine the influence of the polymer dispersity on the fiber formation process the concentration of PiPOx F300 was adjusted to match the viscosity of 25 wt% PiPOx-A315, resulting in a 23.8 wt% solution concentration (Figure S4). The fibers obtained showed a diameter

of 701 ± 104 nm, almost two times higher than the diameter of the fibers obtained from PiPOx-A315. Such a behavior can be explained by the extensibility of the highest molecular weight fractions of a polydisperse polymer which governs the spinnability process as previously mentioned for poly(methyl methacrylate) by Clasen and colleagues.[82] In short, polydisperse polymers generally offer better spinnability than monodisperse polymers with a similar M_n value due to the presence of a higher molar mass fraction.

Further on, the influence of the solvent ratio on the fiber formation process was investigated for PiPOx-F300. Decreasing the H_2O/EtOH mass ratio to 3/7 resulted in the formation of fibers only at 30 wt% concentration (Table S1), whereas at lower concentration no fibers or beaded fibers were obtained. Decreasing the water content even more, e.g. 1/9 H_2O/EtOH, the mass ratio at 20 wt% concentration yielded similar results as the 3/7 mass ratio. Such behavior can be explained by a decrease of the viscosity of the solution with an increasing EtOH fraction, visually evaluated by the vial tilting method (data not shown). Increasing the amount of water in the solvent mixture to 90 or even 100 percent did not allow the formation of stable nanofibers. The polymer solution was much more viscous (visually assessed by vial tilting method) compared to the 1/1 H_2O/EtOH solution leading to an unstable spinning process. In general conclusion, the processing parameters allow tailoring of the fiber diameter to match the needed application. Specifically, the ethanol content of the electrospinning solution can be increased to obtain thicker fiber diameters. However, if smaller diameters are desired, one may conclude that the 1/1 H_2O/EtOH solvent mixture should be used for successful electrospinning of PiPOx, at least for the conditions used in the present study, as it provides the optimal solution viscosity.

2.3. Crosslinking of PiPOx nanofibers

In previous studies, PiPOx was demonstrated to be a versatile polymeric platform for the synthesis of functional materials by making use of the highly effective ring-opening addition reaction of the pendant iPOx rings with carboxylic acids.[64-66, 74-76] Thus, it was hypothesized that water stable PiPOx nanofibers could be easily obtainable by the incorporation of a dicarboxylic acid in the polymer solution prior to the electrospinning, thereby providing a great advantage compared to polymers where additional modification steps are required to introduce the functional groups that are required for crosslinking. Succinic acid was chosen as crosslinker due to its good solubility in the H_2O/ethanol mixture, low toxicity, and bio-based provenience. Succinic acid (10 mol% of COOH to iPOx units) was added to a PiPOx-F300 solution and the mixture was electrospun. Literature indicated that the inclusion of small molecules, if soluble, generally does not significantly influence the electrospinning process and therefore, no influence on the fiber diameter was expected (Figure S5).[81] The crosslinking reaction of PiPOx nanofibers was performed by heating at 120 °C for 5 h. The reaction conditions were chosen based on previous data obtained for modifying PiPOx with (di)carboxylic acids in solution or in swollen particles.[64, 65, 75, 78] Note that in the current study the crosslinking reaction was performed in solid-state at 120 °C avoiding the use of potentially harmful solvents. Furthermore, the high glass-transition temperature (T_g) of PiPOx (177.5 °C) allows the preservation of the nanofibrous morphology during the crosslinking reaction and a wider reaction temperature domain in comparison to other nanofibers obtained from hydrophilic polymers (e.g. PEtOx or PEG) that tend to lose their structural characteristics when heated due to their low T_g or melting temperature (T_m).[65, 78] As analyzed via SEM (Figure S5), the fiber morphology was maintained during the crosslinking reaction, where fiber diameters were obtained of 458 nm ± 91 nm before and 465 ± 79 nm after crosslinking.

To confirm the crosslinking reaction between succinic acid and the PiPOx chains, FTIR spectroscopy was performed for both, non-crosslinked and crosslinked, membranes. These spectra, displayed in **Figure 4**, show the appearance of characteristic peaks at 1727 ($\nu_{C=O}$ ester) and 1540 cm^{-1} ($\nu_{C=N}$ amide II) indicating the ester-amide bond formation as a result of the ring-opening addition reaction confirming the effective crosslinking.

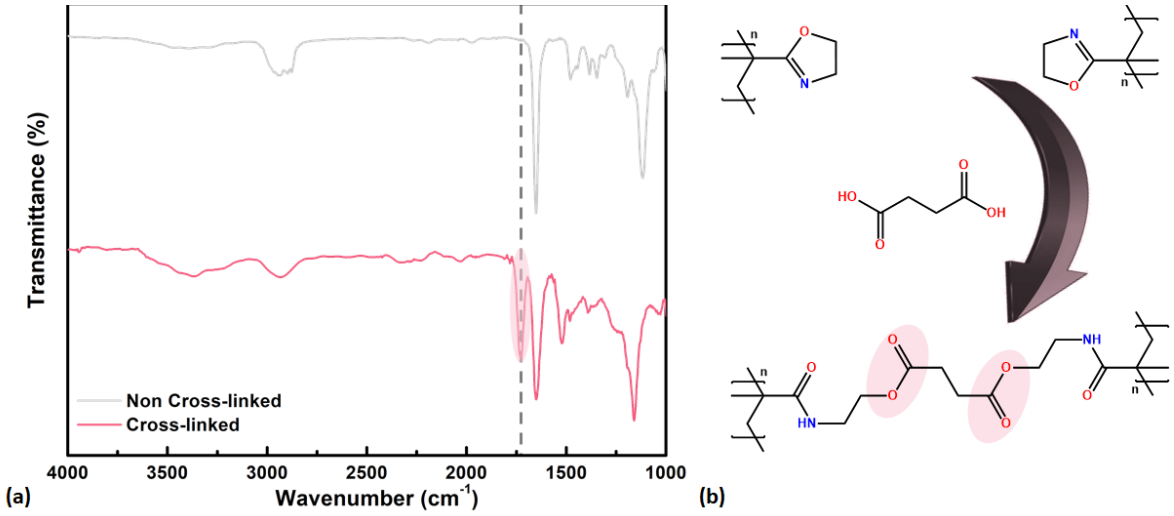

Figure 4. a) FTIR spectra of non-crosslinked (grey) and crosslinked PiPOx nanofiber membranes (red) documenting the obtained crosslinked nanofiber network and its characteristic ester C=O stretch at 1727 cm^{-1}. b) Schematic representation of the crosslinking reaction between two different PiPOx polymer chains and succinic acid, with the indication of the formed esters, emphasized in Red.

To determine the crosslinking density of the obtained PiPOx-based nanofiber network, by FTIR spectroscopy, a calibration curve was constructed from reference copolymers containing known

proportions of propionic acid. In total, six different copolymers were synthesized with varying modification degree from 6 to 60 mol% propionic acid. The modification degree of the copolymers was determined by ^{1}H-NMR spectroscopy (**Figure 5**a). By integrating both the signal of the protons corresponding to the newly formed ester amide structure (–N–CH_2–) at 3.40 ppm and the protons of the unreacted 2-oxazoline ring (=N–CH_2–) at 3.76 ppm, one can easily determine the modification degree. The ^{1}H-NMR spectra indicated that no side-products were formed although the reaction was performed at a relatively high temperature. This SEC analysis of the copolymers revealed a slight increase of the molar mass, as expected, and a steady Đ value for all modified polymers (**Figure 5**b). The copolymers were further analyzed by FTIR spectroscopy, and a calibration curve was obtained by plotting the transmission value corresponding to the ester vibration at 1727 cm^{-1} versus the modification degree calculated from ^{1}H-NMR spectra. The experimental points showed a linear correlation with a high degree of confidence $R^2 = 0.99$ (**Figure 5**c), revealing a T% = 19.04 % degree of modification.

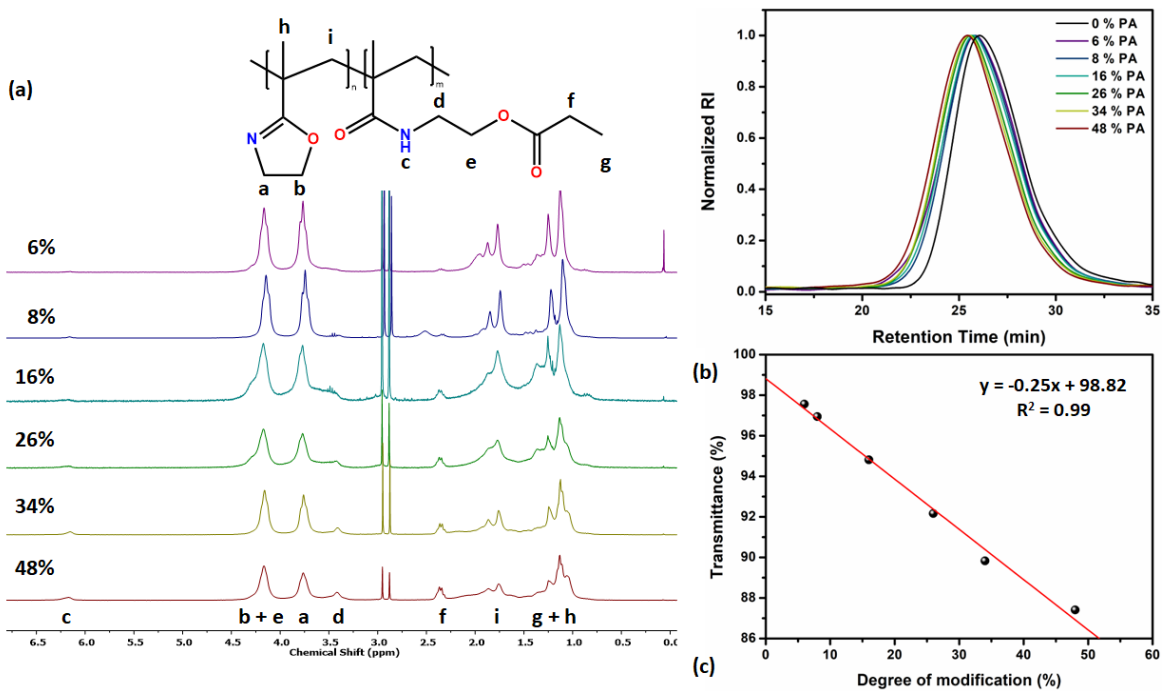

Figure 5. a) ^{1}H NMR spectra in $CDCl_3$ of the PiPOx modified with different degrees of propionic acid; b) corresponding SEC traces for modified copolymers series that show the constant progress of the modification reaction; c) the calibration curve connecting the ester peak intensity from FTIR to the modification degree calculated via ^{1}H NMR showing a linear correlation.

Based on the equation above, a crosslinking efficiency of 99 %, assuming mostly interchain coupling reactions, is found for the PiPOx crosslinked nanofibers with 10 mol% succinic acid, indicating almost full reaction of the succinic acid molecules with the PiPOx network. Thus, the resulting water-stable nanofiber network retained 91.2 % of unreacted, hydrophilic 2-oxazoline groups.

After confirming the efficient crosslinking of the nanofibers by FTIR, we investigated the stability by immersing the crosslinked PiPOx membranes in aqueous environments for different

periods of time. In contrast to non-crosslinked PiPOx nanofibers that instantaneously dissolved when immersed into water, the heat-treated nanofibers did not dissolve and maintained their nanofiber morphology when immersed in water. As such it is clearly demonstrated that water-stable hydrophilic PiPOx nanofibers can be prepared by straightforward crosslinking with succinic acid resulting from the reaction between the pendant 2-oxazoline rings on the polymer structures and the carboxylic acid functionalities of the crosslinker, as illustrated in **Figure 6**. SEM also confirmed the preservation of the nanofibrous structure after immersion of the PiPOx nanofibers in water for 24 hours (**Figure 6**b).

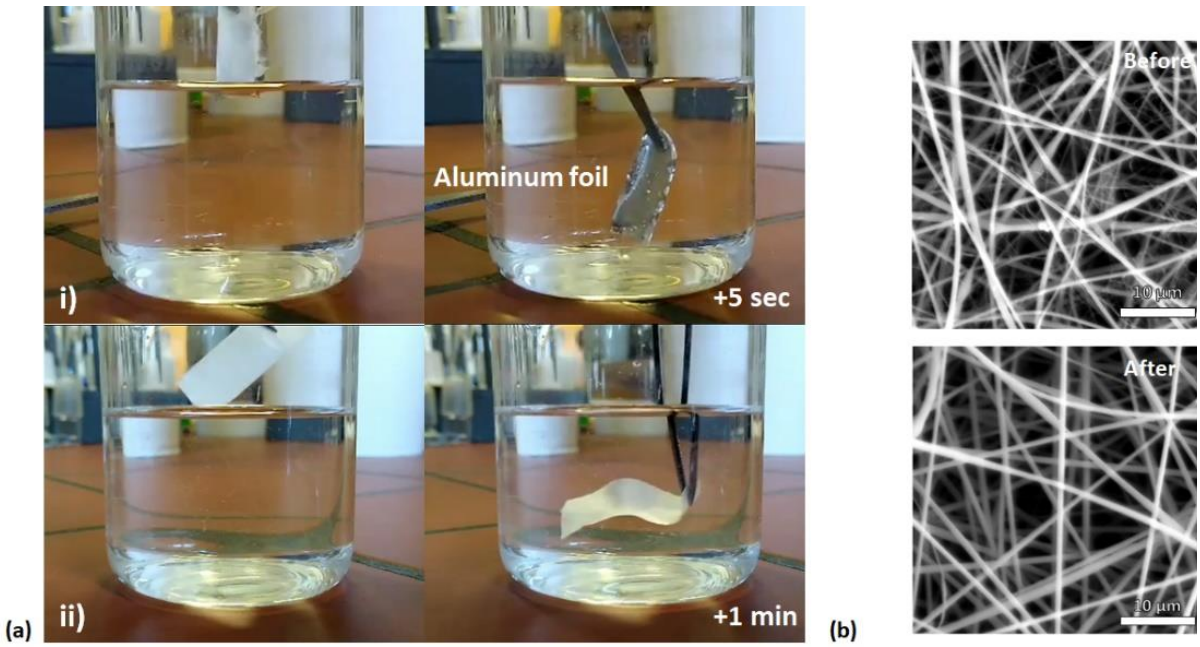

Figure 6. a) Water stability experiment with on top non-crosslinked nanofibers showing the aluminium foil support without the white nanofibrous mat and on the bottom the crosslinked nanofibers after heating showing the presence of the nanofibrous mat after respectively 5

seconds and 1-minute immersion in water. b) SEM analysis of the intact PiPOx crosslinked nanofibers network before and after immersion in water for 24 hours.

2.4. Synthesis of colorimetric sensors based on reactive PiPOx nanofibers

After establishing the straightforward preparation of reactive hydrophilic crosslinked PiPOx nanofiber networks, we focused our attention to the incorporation of carboxylic acid functionalized dyes for continuous food monitoring. The sensor prototype discussed here is envisioned for safeguarding food freshness and edibility by providing a visual and user-friendly read-out via color change. Therefore, a dye toolbox composed of four dyes analyte-responsive dyes was immobilized and evaluated towards actual food samples. The relevant analytes indicative of food spoilage include mainly amines and thiols. Therefore, halochromic and thiol-responsive dyes were selected for incorporation into the crosslinked PiPOx nanofiber material. The selected dyes are the commercially available Disperse Red 1 (pKa = 2.15, Figure S7), Methyl Red (pKa = 5.7, Figure S8), and Ellman's Reagent. Although Disperse Red 1 does not contain a compatible functional handle for covalent attachment to PiPOx, the required carboxylic acid handles was simply introduced by reacting it with succinic anhydride. Furthermore, to cover a more comprehensive pKa range, a fourth dye, HO-azo-COOH, was synthesized with a pKa equal to 8.2 (Figure S9).

In general, due to ease of use, the post-fabrication modification approach for the fabrication of PiPOx-based sensor materials has far more economic potential than a pre-fabrication strategy. The possibility of using a single optimized procedure for the covalent immobilization of different dyes in the PiPOx nanofiber network is more appealing from an application perspective. Therefore, a dye-modification procedure was developed containing three main steps (**Figure 7**). In the first step, the PiPOx nanofiber network is immersed and left to react for five hours in a concentrated

solution of the desired dye at elevated temperatures. Secondly, any residual, non-coupled dye is removed through a continuous washing step. Herein, the residual dye is rinsed away until no color can be observed in the washing solvent. Finally, a quick-drying step of the material is performed to ensure the immobilization of the colorant and remove traces of washing solvent. As this technique is straightforward and accessible, it allows for quick optimization in terms of dye solubility and concentration.

Figure 7. (top) Chemical structures of the selected dyes responsive towards food spoilage metabolites; D1: Ellman's reagent; D2: Methyl Red; D3: acid-functionalized Disperse Red 1; D4: HO-azo-COOH. The pictures show the dye functionalized PiPOx nanofibers before (left) and after (right) exposure to the respective analytes (BT (butanethiol), HCl or TEA (triethylamine) vapor). (bottom) Schematic representation of the post-processing modification protocol for the cross-linked PiPOx fibrous mats.

Successful dye immobilization was evidenced by the retained color of the nanofibrous sensor materials after the extensive washing step (**Figure 7**).

2.5. Proof of concept for food monitoring applications.

The colorimetric response of the dye functionalized PiPOx nanofibers towards each target group of analytes was demonstrated by placing the sensor in a controlled atmosphere containing the desired analyte. The response tests were performed by administering thiols (butanethiol, BT), hydrochloric acid (HCl), and triethylamine (TEA) gasses to Ellman's reagent (D_1), Methyl Red (D_2), Modified Disperse Red 1 (D_3), and HO-azo-COOH (D_4) functionalized PiPOx membranes, respectively. As depicted in **Figure 7**, the results demonstrate that all four dyes have retained their analyte responsiveness after immobilization onto the PiPOx nanofibrous material. Firstly, the **D_1** fibres revealed a color change from white to dark orange after a short period of BT gas exposure. Secondly, the membranes functionalized with **D_2** documented the expected color change from yellow to pink when brought into contact with acidic vapors. Thirdly, the **D_3** membranes showed to be responsive to administered HCl gas as the color transitioned from red to deep purple upon protonation. Finally, the **D_4** membrane was deprotonated after synthesis, exhibiting a yellow color. After protonation with acidic vapors, the membrane exhibited a distinct orange color, which returned to yellow after deprotonation by TEA gas.

As a final proof of concept for the developed continuous food monitoring system based on dye functionalized PiPOx nanofibers, the sensor system was exposed to real-life samples, i.e. cod filets. The design consisted of four different PiPOx nanofiber networks functionalized with the above-described compounds **D_1**, **D_2**, **D_3** and **D_4**. These nanofiber materials were introduced into the head space of the cod and their color was monitored in time. During cod spoilage monitoring over a

time period of ten days, the fibrous networks functionalized with **D_1** and **D_2** documented a significant color change detectable with the naked eye, as depicted in **Figure 8**. The PiPOx nanofibers functionalized with **D_3** and **D_4** did not show a color change. For **D_3** this might be related to an acid-base reaction between the dye and the PiPOx preventing further analyte monitoring. Even though **D_4** depicted a visual color change during initial experiments with TEA gas, no observable difference was noted during the real-life sample investigation. This non-response can be explained due to the high pKa value of 8.7, which requires more alkaline conditions to present its color change.

.

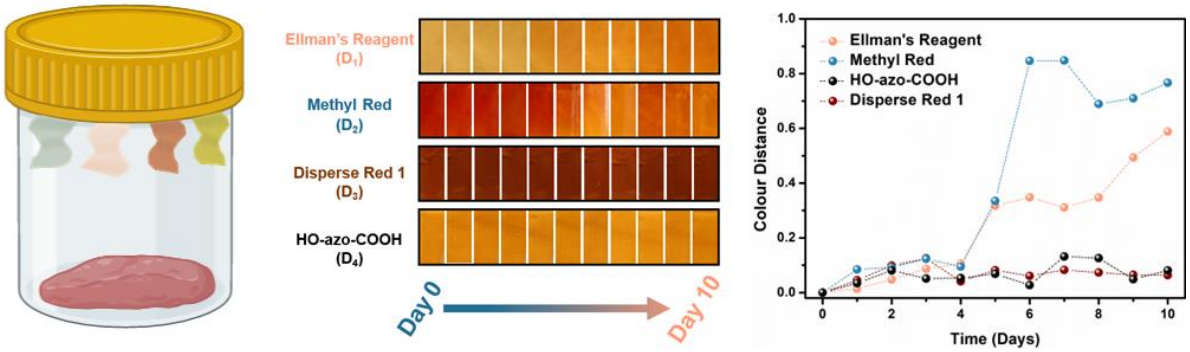

Figure 8. Left: Picture of the set-up for continuous monitoring of cod filet spoilage by dye-functionalized PiPOx nanofibers; Middle: Naked-eye cod spoilage monitoring over 10 days of the four different networks functionalized with D_1, D_2, D_3, and D_4, respectively; Right: Euclidean color distance evolution for the developed sensors with D1, D2, D3, and D4 under cooled conditions, monitored over ten days. Lines were added for visual support only (Note that the package indicated food spoilage after 5 days, which is in agreement with the observed changes).

This visual study was complemented by Euclidean Color Distance (ECD) calculations to further quantify the observed results in function of the color change. This study attempts to provide the first step toward automatizing color analysis through the enhanced ECD formula mentioned above. The color distance can allow objective classification of the analyzed samples using smartphone algorithms. The obtained results, as shown in **Figure 8**, right, display the calculated color distance throughout the different timeframes, always using the initial picture as the reference point.

Initially, as seen from the visual evaluation, until day four, no significant color difference can be observed. However, starting from day five, the ECD values for the two colorants mentioned above, $\mathbf{D_1}$ and $\mathbf{D_2}$, go up drastically to a value of 0.4, indicating a color change due to the formed metabolites. The other colorants document no change in color distance and are thereby confirming the visual evaluation. Important to note that the described expiry date on the packaging of the food samples was expected on experiment day 5, indicating that the PiPOx sensor system is indeed capable of detecting the expected food spoilage time.

As supported by literature, the degradation of proteinaceous food products (e.g., fish and meat) occur in different steps sided by a characteristic change in the headspace above the product.[20, 62, 83] Firstly, the bacterial degradation of sugars and fats occurs, resulting in the production of molecules able to migrate from the meat to the headspace. In this phase, the main volatile organic compounds, VOCs, are dominated by ethanol and free fatty acids, mainly acetic acid. Until this phase lasts, protein foods are considered 'safe products. Only when sugars such as glucose and its direct metabolites are depleted does the breakdown of proteins producing a wide variety of amines, often referred to as the biogenic amines, and sulfur compounds such as thiols. These compounds originate from the breakdown of the proteins' building blocks, the amino acids. By now, the by-products are toxic, and meat consumption at this stage could be a severe hazard. A proper sensing

device can recognize this stage and indicate the potential danger of consuming such a product. The catabolism can potentially explain the reaction observed upon the depicted sensors functionalized with D_1 and D_2, indicating a reaction with the thiol and amine metabolites, respectively. Importantly, these results of the sensor prototype provided the first proof of concept for continuous food spoilage monitoring.

3. Conclusions

In conclusion, we demonstrated a straightforward yet robust procedure to fabricate PiPOx nanofibers with high water stability, which will be of great value towards the development of different functionalized nanofiber platforms, e.g., for tissue engineering or wound dressings. Solvent electrospinning of PiPOx is demonstrated for facile production of narrow nanofibers with excellent tunability from a 1/1 H_2O/EtOH mixture as a green, sustainable solvent system. Moreover, through pendant 2-oxazoline groups in the side chains, the PiPOx membranes were effortlessly crosslinked into the respective nanofibrous networks by introducing a dicarboxylic acid functional molecule during one-pot electrospinning. After a thermal treatment procedure, this resulted in networks with high water stability, whereas a crosslinking efficiency of 99 % was determined. Due to the nature of the polymer itself and the straightforward procedure, we thus introduced a versatile reactive polymer platform without the need for tedious or potentially hazardous chemical modifications, which significantly enhances their applicability for future applications. Within this project the PiPOx platform's reactivity was showcased by the facile functionalization with modified Disperse red 1, with retention of its halochromic properties after post fabrication. Put into a broader context, the reported reactive hydrophilic PiPOx nanofiber networks can be implemented as a hydrophilic base material for various advanced functional

material applications going well beyond the demonstrated sensor applications, including wound dressings, filtration, energy transfer and biomedical imaging.

ASSOCIATED CONTENT

Supporting Information. The supporting material contains the experimental section, supporting Figures S1-S9 and the supporting Table S1.

AUTHOR INFORMATION

Corresponding Author

Richard Hoogenboom − Supramolecular Chemistry Group, Centre of Macromolecular Chemistry (CMaC), Department of Organic and Macromolecular Chemistry, Ghent University, B-9000 Ghent, Belgium. Email: richard.hoogenboom@UGent.be.

Karen de Clerck − Centre for Textile Science and Engineering, Department of Materials, Textiles and Chemical Technology, Ghent University, Tech Lane Science Park 70A, 9052 Ghent, Belgium. E-mail: Karen.DeClerck@UGent.be

Valentin Victor Jerca − Smart Organic Materials Group, "Costin D. Nenitzescu" Institute of Organic and Supramolecular Chemistry, Romanian Academy, Spl. Independentei 202B, 060023, Bucharest, Romania. E-mail: victor.jerca@ccocdn.ro

Author Contributions

The manuscript was written through contributions of all authors. All authors have given approval to the final version of the manuscript.

ACKNOWLEDGMENT

The results in this paper were obtained within the framework of the FWO Strategic Basic Research grants 1S05517N for E.S., 1S89118N for J.B., and 1SA4719N for R.M. A.F.J. and V.V.J. acknowledge the Romanian Ministry of Research, and Innovation and Digitization, CNCS/CCCDI – UEFISCDI for the financial support, project number PN-III-P2-2.1-PED-2021-1776 within PNCDI III. R.H. thanks FWO Flanders and Ghent University for continuous financial support.

REFERENCES

1. Havelaar, A. H.; Kirk, M. D.; Torgerson, P. R.; Gibb, H. J.; Hald, T.; Lake, R. J.; Praet, N.; Bellinger, D. C.; de Silva, N. R.; Gargouri, N.; Speybroeck, N.; Cawthorne, A.; Mathers, C.; Stein, C.; Angulo, F. J.; Devleesschauwer, B.; World Health Organization Foodborne Disease Burden Epidemiology Reference, G. World Health Organization Global Estimates and Regional Comparisons of the Burden of Foodborne Disease in 2010. *PLoS Med* **2015,** 12 (12), e1001923 DOI: 10.1371/journal.pmed.1001923.
2. *Preparatory Study on Food Waste Across Eu*; European Commission: 2010.
3. Ahmed, I.; Lin, H.; Zou, L.; Li, Z.; Brody, A. L.; Qazi, I. M.; Lv, L.; Pavase, T. R.; Khan, M. U.; Khan, S.; Sun, L. An overview of smart packaging technologies for monitoring safety and quality of meat and meat products. *Packaging Technology and Science* **2018,** 31 (7), 449-471 DOI: https://doi.org/10.1002/pts.2380.
4. Wang, S.; Liu, X.; Yang, M.; Zhang, Y.; Xiang, K.; Tang, R. Review of Time Temperature Indicators as Quality Monitors in Food Packaging. *Packaging Technology and Science* **2015,** 28 (10), 839-867 DOI: https://doi.org/10.1002/pts.2148.
5. Mills, A.; Hawthorne, D.; Graham, A.; Lawrie, K. Novel time-temperature and 'consume-within' indicator based on gas-diffusion. *Chemical Communications* **2016,** 52 (97), 13987-13990 DOI: 10.1039/C6CC07906G.
6. Gil, L.; Barat, J. M.; Escriche, I.; Garcia-Breijo, E.; Martínez-Máñez, R.; Soto, J. An electronic tongue for fish freshness analysis using a thick-film array of electrodes. *Microchimica Acta* **2008,** 163 (1), 121-129 DOI: 10.1007/s00604-007-0934-5.
7. Cetó, X.; Voelcker, N. H.; Prieto-Simón, B. Bioelectronic tongues: New trends and applications in water and food analysis. *Biosensors and Bioelectronics* **2016,** 79, 608-626 DOI: https://doi.org/10.1016/j.bios.2015.12.075.
8. Wojnowski, W.; Majchrzak, T.; Dymerski, T.; Gębicki, J.; Namieśnik, J. Electronic noses: Powerful tools in meat quality assessment. *Meat Science* **2017,** 131, 119-131 DOI: https://doi.org/10.1016/j.meatsci.2017.04.240.
9. Chen, Q.; Hui, Z.; Zhao, J.; Ouyang, Q. Evaluation of chicken freshness using a low-cost colorimetric sensor array with AdaBoost–OLDA classification algorithm. *LWT - Food Science and Technology* **2014,** 57 (2), 502-507 DOI: https://doi.org/10.1016/j.lwt.2014.02.031.

10. Kuswandi, B.; Nurfawaidi, A. On-package dual sensors label based on pH indicators for real-time monitoring of beef freshness. *Food Control* **2017,** 82, 91-100 DOI: https://doi.org/10.1016/j.foodcont.2017.06.028.
11. Dudnyk, I.; Janeček, E.-R.; Vaucher-Joset, J.; Stellacci, F. Edible sensors for meat and seafood freshness. *Sensors and Actuators B: Chemical* **2018,** 259, 1108-1112 DOI: https://doi.org/10.1016/j.snb.2017.12.057.
12. Ding, L.; Li, X.; Hu, L.; Zhang, Y.; Jiang, Y.; Mao, Z.; Xu, H.; Wang, B.; Feng, X.; Sui, X. A naked-eye detection polyvinyl alcohol/cellulose-based pH sensor for intelligent packaging. *Carbohydrate Polymers* **2020,** 233, 115859 DOI: https://doi.org/10.1016/j.carbpol.2020.115859.
13. Liu, B.; Gurr, P. A.; Qiao, G. G. Irreversible Spoilage Sensors for Protein-Based Food. *ACS Sensors* **2020,** 5 (9), 2903-2908 DOI: 10.1021/acssensors.0c01211.
14. Zhang, H.; Hou, A.; Xie, K.; Gao, A. Smart color-changing paper packaging sensors with pH sensitive chromophores based on azo-anthraquinone reactive dyes. *Sensors and Actuators B: Chemical* **2019,** 286, 362-369 DOI: https://doi.org/10.1016/j.snb.2019.01.165.
15. Salinas, Y.; Ros-Lis, J. V.; Vivancos, J.-L.; Martínez-Máñez, R.; Marcos, M. D.; Aucejo, S.; Herranz, N.; Lorente, I.; Garcia, E. A novel colorimetric sensor array for monitoring fresh pork sausages spoilage. *Food Control* **2014,** 35 (1), 166-176 DOI: https://doi.org/10.1016/j.foodcont.2013.06.043.
16. Pacquit, A.; Frisby, J.; Diamond, D.; Lau, K. T.; Farrell, A.; Quilty, B.; Diamond, D. Development of a smart packaging for the monitoring of fish spoilage. *Food Chemistry* **2007,** 102 (2), 466-470 DOI: https://doi.org/10.1016/j.foodchem.2006.05.052.
17. O'Halloran, G. R.; Troy, D. J.; Buckley, D. J. The relationship between early post-mortem pH and the tenderisation of beef muscles. *Meat Science* **1997,** 45 (2), 239-251 DOI: https://doi.org/10.1016/S0309-1740(96)00074-5.
18. Pacquit, A.; Lau, K. T.; McLaughlin, H.; Frisby, J.; Quilty, B.; Diamond, D. Development of a volatile amine sensor for the monitoring of fish spoilage. *Talanta* **2006,** 69 (2), 515-520 DOI: https://doi.org/10.1016/j.talanta.2005.10.046.
19. Sirocchi, V.; Caprioli, G.; Ricciutelli, M.; Vittori, S.; Sagratini, G. Simultaneous determination of ten underivatized biogenic amines in meat by liquid chromatography-tandem mass spectrometry (HPLC-MS/MS). *Journal of Mass Spectrometry* **2014,** 49 (9), 819-825 DOI: https://doi.org/10.1002/jms.3418.
20. Vinci, G.; Antonelli, M. L. Biogenic amines: quality index of freshness in red and white meat. *Food Control* **2002,** 13 (8), 519-524 DOI: https://doi.org/10.1016/S0956-7135(02)00031-2.
21. Crowley, K.; Pacquit, A.; Hayes, J.; King Tong, L.; Diamond, D. In *A gas-phase colorimetric sensor for the detection of amine spoilage products in packaged fish*, SENSORS, 2005 IEEE, 30 Oct.-3 Nov. 2005, 2005; 2005; p 4 pp.
22. Biesuz, R.; Quadrelli, P.; Magnaghi, L. R. Sensors for the Evaluation of the Quality of Meat-Based Food. US6833408B22020.
23. Biesuz, R.; Quadrelli, P.; Magnaghi, L. R. Sensori per la Valutazione della Qualità di Prodotti Alimentari a Base di Carne. 10201900000464, 2019.
24. Yousefi, H.; Su, H.-M.; Imani, S. M.; Alkhaldi, K.; M. Filipe, C. D.; Didar, T. F. Intelligent Food Packaging: A Review of Smart Sensing Technologies for Monitoring Food Quality. *ACS Sensors* **2019,** 4 (4), 808-821 DOI: 10.1021/acssensors.9b00440.

25. Chalitangkoon, J.; Monvisade, P. Synthesis of chitosan-based polymeric dyes as colorimetric pH-sensing materials: Potential for food and biomedical applications. *Carbohydrate Polymers* **2021,** 260, 117836 DOI: https://doi.org/10.1016/j.carbpol.2021.117836.
26. Anton, F. Process and apparatus for preparing artificial threads. US Patent No. 1975504, 1934.
27. Yarin, A. L.; Koombhongse, S.; Reneker, D. H. Bending instability in electrospinning of nanofibers. *Journal of Applied Physics* **2001,** 89 (5), 3018-3026 DOI: 10.1063/1.1333035.
28. Reneker, D. H.; Yarin, A. L.; Fong, H.; Koombhongse, S. Bending instability of electrically charged liquid jets of polymer solutions in electrospinning. *Journal of Applied Physics* **2000,** 87 (9), 4531-4547 DOI: 10.1063/1.373532.
29. Dahlin, R. L.; Kasper, F. K.; Mikos, A. G. Polymeric Nanofibers in Tissue Engineering. *Tissue Engineering Part B: Reviews* **2011,** 17 (5), 349-364 DOI: 10.1089/ten.teb.2011.0238.
30. Pham, Q. P.; Sharma, U.; Mikos, A. G. Electrospinning of Polymeric Nanofibers for Tissue Engineering Applications: A Review. *Tissue Engineering* **2006,** 12 (5), 1197-1211 DOI: 10.1089/ten.2006.12.1197.
31. Vasita, R.; Katti, D. S. Nanofibers and their applications in tissue engineering. *International journal of nanomedicine* **2006,** 1 (1), 15-30 DOI: 10.2147/nano.2006.1.1.15.
32. Dhineshbabu, N. R.; Karunakaran, G.; Suriyaprabha, R.; Manivasakan, P.; Rajendran, V. Electrospun MgO/Nylon 6 Hybrid Nanofibers for Protective Clothing. *Nano-Micro Letters* **2014,** 6 (1), 46-54 DOI: 10.1007/BF03353768.
33. Gorji, M.; Bagherzadeh, R.; Fashandi, H., 21 - Electrospun nanofibers in protective clothing. In *Electrospun Nanofibers*, Afshari, M., Ed. Woodhead Publishing: 2017; pp 571-598.
34. Balusamy, B.; Senthamizhan, A.; Uyar, T. Functionalized Electrospun Nanofibers as a Versatile Platform for Colorimetric Detection of Heavy Metal Ions in Water: A Review. *Materials* **2020,** 13 (10), 2421 DOI: 10.3390/ma13102421.
35. Ding, R.; Luo, Z.; Ma, X.; Fan, X.; Xue, L.; Lin, X.; Chen, S. High Sensitive Sensor Fabricated by Reduced Graphene Oxide/Polyvinyl Butyral Nanofibers for Detecting Cu (II) in Water. *International Journal of Analytical Chemistry* **2015,** 2015, 723276 DOI: 10.1155/2015/723276.
36. Schoolaert, E.; Hoogenboom, R.; De Clerck, K. Colorimetric Nanofibers as Optical Sensors. *Advanced Functional Materials* **2017,** 27 (38), 1702646 DOI: https://doi.org/10.1002/adfm.201702646.
37. Valdez, M.; Gupta, S. K.; Lozano, K.; Mao, Y. ForceSpun polydiacetylene nanofibers as colorimetric sensor for food spoilage detection. *Sensors and Actuators B: Chemical* **2019,** 297, 126734 DOI: https://doi.org/10.1016/j.snb.2019.126734.
38. Yapor, J. P.; Alharby, A.; Gentry-Weeks, C.; Reynolds, M. M.; Alam, A. K. M. M.; Li, Y. V. Polydiacetylene Nanofiber Composites as a Colorimetric Sensor Responding To Escherichia coli and pH. *ACS Omega* **2017,** 2 (10), 7334-7342 DOI: 10.1021/acsomega.7b01136.
39. Babel, A.; Li, D.; Xia, Y.; Jenekhe, S. A. Electrospun Nanofibers of Blends of Conjugated Polymers: Morphology, Optical Properties, and Field-Effect Transistors. *Macromolecules* **2005,** 38 (11), 4705-4711 DOI: 10.1021/ma047529r.
40. Lou, L.-H.; Qin, X.-H.; Zhang, H. Preparation and study of low-resistance polyacrylonitrile nano membranes for gas filtration. *Textile Research Journal* **2016,** 87 (2), 208-215 DOI: 10.1177/0040517515627171.

41. Bhardwaj, N.; Kundu, S. C. Electrospinning: A fascinating fiber fabrication technique. *Biotechnology Advances* **2010,** 28 (3), 325-347 DOI: https://doi.org/10.1016/j.biotechadv.2010.01.004.
42. Jiang, S.; Hou, H.; Agarwal, S.; Greiner, A. Polyimide Nanofibers by "Green" Electrospinning via Aqueous Solution for Filtration Applications. *ACS Sustainable Chemistry & Engineering* **2016,** 4 (9), 4797-4804 DOI: 10.1021/acssuschemeng.6b01031.
43. Chen, L.; Zhu, C.; Fan, D.; Liu, B.; Ma, X.; Duan, Z.; Zhou, Y. A human-like collagen/chitosan electrospun nanofibrous scaffold from aqueous solution: Electrospun mechanism and biocompatibility. *Journal of Biomedical Materials Research Part A* **2011,** 99A (3), 395-409 DOI: https://doi.org/10.1002/jbm.a.33202.
44. Chen, C.; Chuanbao, C.; Xilan, M.; Yin, T.; Hesun, Z. Preparation of non-woven mats from all-aqueous silk fibroin solution with electrospinning method. *Polymer* **2006,** 47 (18), 6322-6327 DOI: https://doi.org/10.1016/j.polymer.2006.07.009.
45. Lu, W.; Ma, M.; Xu, H.; Zhang, B.; Cao, X.; Guo, Y. Gelatin nanofibers prepared by spiral-electrospinning and cross-linked by vapor and liquid-phase glutaraldehyde. *Materials Letters* **2015,** 140, 1-4 DOI: https://doi.org/10.1016/j.matlet.2014.10.146.
46. Shi, J. J.; Yang, E. L. Green Electrospinning and Crosslinking of Polyvinyl Alcohol/Citric Acid. *Journal of Nano Research* **2015,** 32, 32-42 DOI: 10.4028/www.scientific.net/JNanoR.32.32.
47. Ge, J. C.; Wu, G.; Yoon, S. K.; Kim, M. S.; Choi, N. J. Study on the Preparation and Lipophilic Properties of Polyvinyl Alcohol (PVA) Nanofiber Membranes via Green Electrospinning. *Nanomaterials* **2021,** 11 (10), 2514 DOI: 10.3390/nano11102514.
48. Golba, B.; Kalaoglu-Altan, O. I.; Sanyal, R.; Sanyal, A. Hydrophilic Cross-Linked Polymeric Nanofibers Using Electrospinning: Imparting Aqueous Stability to Enable Biomedical Applications. *ACS Applied Polymer Materials* **2022,** 4 (1), 1-17 DOI: 10.1021/acsapm.1c01286.
49. Zhong, T.; Liu, W.; Liu, H. Green electrospinning of chitin propionate to manufacture nanofiber mats. *Carbohydrate Polymers* **2021,** 273, 118593 DOI: https://doi.org/10.1016/j.carbpol.2021.118593.
50. Thamer, B. M.; Al-Sabri, A. E.; Almansob, A.; El-Newehy, M. H. Fabrication of Biohybrid Nanofibers by the Green Electrospinning Technique and Their Antibacterial Activity. *ACS Omega* **2022,** 7 (8), 7311-7319 DOI: 10.1021/acsomega.1c07141.
51. Sun, J.; Bubel, K.; Chen, F.; Kissel, T.; Agarwal, S.; Greiner, A. Nanofibers by Green Electrospinning of Aqueous Suspensions of Biodegradable Block Copolyesters for Applications in Medicine, Pharmacy and Agriculture. *Macromolecular Rapid Communications* **2010,** 31 (23), 2077-2083 DOI: https://doi.org/10.1002/marc.201000379.
52. ÇALLIOĞLU, F. C.; GÜLER, H. K. Fabrication of Polyvinylpyrrolidone Nanofibers with Green Solvents. *Süleyman Demirel Üniversitesi Fen Edebiyat Fakültesi Fen Dergisi* **2019,** 14 (2), 352-366.
53. Kalaoglu-Altan, O. I.; Verbraeken, B.; Lava, K.; Gevrek, T. N.; Sanyal, R.; Dargaville, T.; De Clerck, K.; Hoogenboom, R.; Sanyal, A. Multireactive Poly(2-oxazoline) Nanofibers through Electrospinning with Crosslinking on the Fly. *ACS Macro Letters* **2016,** 5 (6), 676-681 DOI: 10.1021/acsmacrolett.6b00188.
54. Wei, L.; Xiao, L.; He, Y. Synthesis of water soluble silver-nanoparticle-embedded polymer nanofibers with poly(2-ethyl-2-oxazoline) by a straightforward polyol process. *Journal of Materials Research* **2011,** 26 (13), 1614-1620 DOI: 10.1557/jmr.2011.174.

55. Schoolaert, E.; Ryckx, P.; Geltmeyer, J.; Maji, S.; Van Steenberge, P. H. M.; D'hooge, D. R.; Hoogenboom, R.; De Clerck, K. Waterborne Electrospinning of Poly(N-isopropylacrylamide) by Control of Environmental Parameters. *ACS Applied Materials & Interfaces* **2017,** 9 (28), 24100-24110 DOI: 10.1021/acsami.7b05074.
56. Li, Y.; Vergaelen, M.; Schoolaert, E.; Hoogenboom, R.; De Clerck, K. Effect of crosslinking stage on photocrosslinking of benzophenone functionalized poly(2-ethyl-2-oxazoline) nanofibers obtained by aqueous electrospinning. *European Polymer Journal* **2019,** 112, 24-30 DOI: https://doi.org/10.1016/j.eurpolymj.2018.12.030.
57. Yoshida, H.; Klinkhammer, K.; Matsusaki, M.; Möller, M.; Klee, D.; Akashi, M. Disulfide-Crosslinked Electrospun Poly(γ-glutamic acid) Nonwovens as Reduction-Responsive Scaffolds. *Macromolecular Bioscience* **2009,** 9 (6), 568-574 DOI: https://doi.org/10.1002/mabi.200800334.
58. Geltmeyer, J.; De Roo, J.; Van den Broeck, F.; Martins, J. C.; De Buysser, K.; De Clerck, K. The influence of tetraethoxysilane sol preparation on the electrospinning of silica nanofibers. *Journal of Sol-Gel Science and Technology* **2016,** 77 (2), 453-462 DOI: 10.1007/s10971-015-3875-1.
59. Destaye, A. G.; Lin, C.-K.; Lee, C.-K. Glutaraldehyde Vapor Cross-linked Nanofibrous PVA Mat with in Situ Formed Silver Nanoparticles. *ACS Applied Materials & Interfaces* **2013,** 5 (11), 4745-4752 DOI: 10.1021/am401730x.
60. Drexler, J. W.; Powell, H. M. Dehydrothermal Crosslinking of Electrospun Collagen. *Tissue Engineering Part C: Methods* **2010,** 17 (1), 9-17 DOI: 10.1089/ten.tec.2009.0754.
61. Jiang, S.; Liu, F.; Lerch, A.; Ionov, L.; Agarwal, S. Unusual and Superfast Temperature-Triggered Actuators. *Advanced Materials* **2015,** 27 (33), 4865-4870 DOI: https://doi.org/10.1002/adma.201502133.
62. Vargas-Osorio, Z.; Ruther, F.; Chen, S.; Sengupta, S.; Liverani, L.; Michálek, M.; Galusek, D.; Boccaccini, A. R. Environmentally friendly fabrication of electrospun nanofibers made of polycaprolactone, chitosan and κ-carrageenan (PCL/CS/κ-C). *Biomedical Materials* **2022,** 17 (4), 045019 DOI: 10.1088/1748-605X/ac6eaa.
63. Stubbe, B.; Li, Y.; Vergaelen, M.; Van Vlierberghe, S.; Dubruel, P.; De Clerck, K.; Hoogenboom, R. Aqueous electrospinning of poly(2-ethyl-2-oxazoline): Mapping the parameter space. *European Polymer Journal* **2017,** 88, 724-732 DOI: https://doi.org/10.1016/j.eurpolymj.2016.09.014.
64. Jerca, F. A.; Anghelache, A. M.; Ghibu, E.; Cecoltan, S.; Stancu, I.-C.; Trusca, R.; Vasile, E.; Teodorescu, M.; Vuluga, D. M.; Hoogenboom, R.; Jerca, V. V. Poly(2-isopropenyl-2-oxazoline) Hydrogels for Biomedical Applications. *Chemistry of Materials* **2018,** 30 (21), 7938-7949 DOI: 10.1021/acs.chemmater.8b03545.
65. Jerca, F. A.; Jerca, V. V.; Anghelache, A. M.; Vuluga, D. M.; Hoogenboom, R. Poly(2-isopropenyl-2-oxazoline) as a versatile platform towards thermoresponsive copolymers. *Polymer Chemistry* **2018,** 9 (25), 3473-3478 DOI: 10.1039/C8PY00612A.
66. Jerca, F. A.; Jerca, V. V.; Hoogenboom, R. In Vitro Assessment of the Hydrolytic Stability of Poly(2-isopropenyl-2-oxazoline). *Biomacromolecules* **2021,** 22 (12), 5020-5032 DOI: 10.1021/acs.biomac.1c00994.
67. Jerca, V. V.; Nicolescu, F. A.; Trusca, R.; Vasile, E.; Baran, A.; Anghel, D. F.; Vasilescu, D. S.; Vuluga, D. M. Oxazoline-functional polymer particles graft with azo-dye. *Reactive and Functional Polymers* **2011,** 71 (4), 373-379 DOI: https://doi.org/10.1016/j.reactfunctpolym.2010.12.004.

68. Weber, C.; Neuwirth, T.; Kempe, K.; Ozkahraman, B.; Tamahkar, E.; Mert, H.; Becer, C. R.; Schubert, U. S. 2-Isopropenyl-2-oxazoline: A Versatile Monomer for Functionalization of Polymers Obtained via RAFT. *Macromolecules* **2012,** 45 (1), 20-27 DOI: 10.1021/ma2021387.
69. Raus, V.; Hološ, A.; Kronek, J.; Mosnáček, J. Well-Defined Linear and Grafted Poly(2-isopropenyl-2-oxazoline)s Prepared via Copper-Mediated Reversible-Deactivation Radical Polymerization Methods. *Macromolecules* **2020,** 53 (6), 2077-2087 DOI: 10.1021/acs.macromol.9b02662.
70. Zhang, N.; Salzinger, S.; Soller, B. S.; Rieger, B. Rare Earth Metal-Mediated Group-Transfer Polymerization: From Defined Polymer Microstructures to High-Precision Nano-Scaled Objects. *Journal of the American Chemical Society* **2013,** 135 (24), 8810-8813 DOI: 10.1021/ja4036175.
71. Feng, H.; Changez, M.; Hong, K.; Mays, J. W.; Kang, N.-G. 2-Isopropenyl-2-oxazoline: Well-Defined Homopolymers and Block Copolymers via Living Anionic Polymerization. *Macromolecules* **2017,** 50 (1), 54-62 DOI: 10.1021/acs.macromol.6b02084.
72. Xu, X.; Jerca, F. A.; Van Hecke, K.; Jerca, V. V.; Hoogenboom, R. High compression strength single network hydrogels with pillar[5]arene junction points. *Materials Horizons* **2020,** 7 (2), 566-573 DOI: 10.1039/C9MH01401B.
73. Cegłowski, M.; Jerca, V. V.; Jerca, F. A.; Hoogenboom, R. Reduction-Responsive Molecularly Imprinted Poly(2-isopropenyl-2-oxazoline) for Controlled Release of Anticancer Agents. *Pharmaceutics* **2020,** 12 (6), 506 DOI: 10.3390/pharmaceutics12060506.
74. Xu, X.; Jerca, F. A.; Jerca, V. V.; Hoogenboom, R. Covalent Poly(2-Isopropenyl-2-Oxazoline) Hydrogels with Ultrahigh Mechanical Strength and Toughness through Secondary Terpyridine Metal-Coordination Crosslinks. *Advanced Functional Materials* **2019,** 29 (48), 1904886 DOI: https://doi.org/10.1002/adfm.201904886.
75. Spiridon, M. C.; Jerca, F. A.; Jerca, V. V.; Vasilescu, D. S.; Vuluga, D. M. 2-Oxazoline based photo-responsive azo-polymers. Synthesis, characterization and isomerization kinetics. *European Polymer Journal* **2013,** 49 (2), 452-463 DOI: https://doi.org/10.1016/j.eurpolymj.2012.11.024.
76. Leiske, M. N.; Mahmoud, A. M.; Warne, N. M.; Goos, J. A. C. M.; Pascual, S.; Montembault, V.; Fontaine, L.; Davis, T. P.; Whittaker, M. R.; Kempe, K. Poly(2-isopropenyl-2-oxazoline) – a structural analogue to poly(vinyl azlactone) with Orthogonal Reactivity. *Polymer Chemistry* **2020,** 11 (35), 5681-5692 DOI: 10.1039/D0PY00861C.
77. Kopka, B.; Kost, B.; Basko, M. Poly(2-isopropenyl-2-oxazoline) as a reactive polymer for materials development. *Polymer Chemistry* **2022,** 13 (33), 4736-4746 DOI: 10.1039/D2PY00660J.
78. Jerca, V. V.; Nicolescu, F. A.; Baran, A.; Anghel, D. F.; Vasilescu, D. S.; Vuluga, D. M. Synthesis and characterization of side-chain oxazoline–methyl methacrylate copolymers bearing azo-dye. *Reactive and Functional Polymers* **2010,** 70 (10), 827-835 DOI: https://doi.org/10.1016/j.reactfunctpolym.2010.07.018.
79. Zhang, N.; Huber, S.; Schulz, A.; Luxenhofer, R.; Jordan, R. Cylindrical Molecular Brushes of Poly(2-oxazoline)s from 2-Isopropenyl-2-oxazoline. *Macromolecules* **2009,** 42 (6), 2215-2221 DOI: 10.1021/ma802627y.
80. Ying, Q.; Chu, B. Overlap concentration of macromolecules in solution. *Macromolecules* **1987,** 20 (2), 362-366 DOI: 10.1021/ma00168a023.

81. Van der Schueren, L.; Mollet, T.; Ceylan, Ö.; De Clerck, K. The development of polyamide 6.6 nanofibres with a pH-sensitive function by electrospinning. *European Polymer Journal* **2010,** 46 (12), 2229-2239 DOI: https://doi.org/10.1016/j.eurpolymj.2010.09.016.
82. Palangetic, L.; Reddy, N. K.; Srinivasan, S.; Cohen, R. E.; McKinley, G. H.; Clasen, C. Dispersity and spinnability: Why highly polydisperse polymer solutions are desirable for electrospinning. *Polymer* **2014,** 55 (19), 4920-4931 DOI: https://doi.org/10.1016/j.polymer.2014.07.047.
83. Raffaela, B.; Lisa Rita, M., Role of Biogenic Amines in Protein Foods Sensing: Myths and Evidence. In *Meat and Nutrition*, Chhabi Lal, R., Ed. IntechOpen: Rijeka, 2021; p Ch. 6.

TOC GRAPHIC: